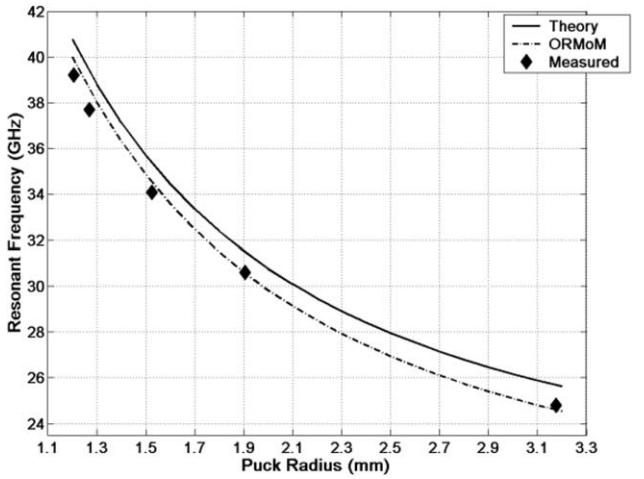

Figure 4 Computed and measured data for the resonator

Figure 4 displays computed and measured data of the resonant frequencies for several radii of the dielectric resonator with dimensions stated earlier. The resonant frequencies were measured on a network analyzer using a two-port loop coupling system with pucks of five radii, 1.206, 1.27, 1.524, 1.905, and 3.175 mm [10]. All the resonators had the same length, $L = 2.4$ mm. The theoretical result from Eq. (5) is compared to ORMoM computation and the measured resonant frequency, plotted as a function of the puck radius in Figure 4. For a fixed length, the radius inversely affects the resonant frequency. At the smallest radius of 1.2 mm, the discrepancy between theory and ORMoM is about 2%, but at the larger radius of 3.2 mm, it is about 6%. The higher margin of discrepancy is due to the fact that the plate size, b, is not considered in Eq. (5). The plates are assumed to be infinite in theory, while the MoM computation and the measurements deal with a plate radius $b = 5$ mm. At this radius, we have analytically determined that practically all of the stored energy is confined to the dielectric, so that the quality factor is the highest possible for the range of puck radius, a, selected in Figure 4 [10]. However, there is still some fringing loss associated with the resonator, which is not accounted in the theoretical model, but considered accurately both in MoM and the measurements. The theoretical assumption of infinite endplate size becomes worse for the larger radii in Figure 4, because of proximity interaction between puck and the plates. Therefore, it is not surprising that the measured data agree closely with the MoM computation, but not with the theoretical model. We have also investigated the resonance of a dielectric sphere using triangular patch code [13] and ORMoM. We have observed excellent corroboration between the Mie series solution and our computation. These results are not presented for brevity.

4. SUMMARY

We have presented an order-recursive moment method for the swept-frequency resonance analysis of arbitrary structures, using LU decomposition of an augmented linear system comprising the moments. In comparison with existing approaches to solving the linear systems in MoM, ORMoM avoids repetitive matrix operations by properly partitioning the geometry such that the increasing cell resolution necessary at higher frequencies produces an augmented system, which can be solved efficiently using the solution at the previous step. The method has been applied to the analysis of resonances on a square plate and a parallel plate dielectric cylinder. Good corroboration of the resonant frequencies of the latter with measured data validates the proposed swept-frequency ORMoM.

REFERENCES

1. R.F. Harrington, Field computation by moment methods, Macmillan, New York, NY, 1968.
2. em, Sonnet Software. Available at: http://www.sonnetsoftware.com/
3. FEKO, EM Software & Systems. Available at: http://www.feko.info/
4. HFSS Integral Equation Solver (HFSS-IE), ANSYS. Available at: www.ansys.com.
5. Momentum, Agilent Technologies. Available at: http://www.home.agilent.com/en/pc-1887116/momentum-3d-planar-em-simulator?&cc=US&lc=eng.
6. P. Misra and K. Naishadham, Order recursive Gaussian elimination (ORGE) and efficient CAD of microwave circuits, IEEE Trans Microwave Theory Tech 44 (1996), 2166–1273.
7. K. Naishadham and P. Misra, Order recursive method of moments (ORMoM) for iterative design applications, IEEE Trans Microwave Theory Tech 44 (1996), 2595–2604.
8. K. Naishadham, T.W. Nuteson, and R. Mittra, Parametric interpolation of the moment matrix in a mixed potential surface integral equation formulation, Int J Microwave Millimeter Wave Comput-Aided Eng 9 (1999), 474–489.
9. C.E. Baum, The singularity expansion method, In: L.B. Felsen, (Ed.), Transient electromagnetic fields, Springer-Verlag, 1976.
10. E.K. Moser and K. Naishadham, Dielectric resonators as microwave characterization tools, IEEE Trans Appl Supercond 7 (1997), 2018–2021.
11. J.R. Mautz and R.F. Harrington, Radiation and scattering from bodies of revolution. Appl Sci Res 20 (1969), 405–435.
12. D. Kajfez and P. Guillon, (Eds.), Dielectric resonators, Artech House, Norwood, MA, 1986, 65–111.
13. K. Umashanker, A. Taflove, and S.M. Rao, Electromagnetic scattering by arbitrary shaped three-dimensional homogenous dielectric objects, IEEE Trans Antennas Propag AP-34 (1986), 758–765.

SWITCHABLE AND TUNABLE MICROWAVE PHOTONIC FILTER BASED ON REFLECTIVE SEMICONDUCTOR OPTICAL AMPLIFIER

Enming Xu,[1] Fei Wang,[2] and Peili Li[1]
[1] School of Opto-Electronic Engineering, Nanjing University of Posts and Telecommunications, Nanjing 210023, China; Corresponding author: enmingxu@njupt.edu.cn
[2] School of Optoelectronic Information, Chongqing University of Technology, Chongqing 400054, China

Received 16 May 2013

ABSTRACT: *A microwave photonic filter, which can be switched between a high-Q bandpass filter and a notch filter, is proposed and experimentally demonstrated. It is based on a recirculating delay line loop with a reflective semiconductor optical amplifier, and negative taps are generated employing wavelength conversion. The filter can be also tuned by adjusting an optical variable delay line.* © 2014 Wiley Periodicals, Inc. Microwave Opt Technol Lett 56:198–201, 2014; View this article online at wileyonlinelibrary.com. DOI 10.1002/mop.28067

Key words: *microwave filter; microwave photonic; optical signal processing; reflective semiconductor optical amplifier*

1. INTRODUCTION

Using photonic approaches to process microwave and radio frequency (RF) signals is attractive due to the inherent advantages such as low loss, broad bandwidth, immunity to electromagnetic

interference (EMI), the possibility of good tunability, and reconfigurability [1–3]. Furthermore, photonic signal processing of microwave signals has the potential advantages of overcoming the existing electronic bottlenecks and provides functions in microwave systems that are very complex or even impossible to be carried out using pure electronic devices.

Many microwave photonic filter structures have been proposed to realize either bandpass filters [4–6] or notch filters with flat passband [7–9]. However, these proposed filters cannot be switched between a bandpass filter and a notch filter, which can greatly increase the flexibility in applications. Few filters switched between a high-Q bandpass filter and a notch filter with flat passband have been proposed, such as using a phase modulator and two tunable optical filters [10] or using a 2×1 Mach–Zehnder modulator (MZM) with two different wavelength optical sources to generate two 180° RF phase difference modulated optical signals [11]. However, these proposed switchable filters are not based on a common MZM, which is widely used in many applications. Weiwei Zhang et al. [12] proposed a switchable filter based on a common MZM and a dual-drive Mach–Zehnder modulator (DDMZM) using stimulated Brillouin scattering (SBS). The scheme exhibits a complex structure, and the bandwidth of frequency response is limited by the SBS gain bandwidth.

In this article, we propose and demonstrate a novel microwave photonic filter, which can be switched between a high-Q bandpass filter and a notch filter with flat passband. It is based on a common MZM using a recirculating delay line (RDL) loop. The RDL loop comprises a reflective semiconductor optical amplifier (RSOA) and an optical bandpass filter (OBF). Converted signal serving as a negative tap is generated using cross-gain modulation (XGM) of the amplified spontaneous emission (ASE) of the RSOA. The transfer function of the microwave photonic filter can be switched by changing output port of the RDL loop. The microwave photonic filter can also be tuned by adjusting an optical variable delay line (OVDL).

2. OPERATION PRINCIPLE AND EXPERIMENTAL SETUP

The schematic diagram of the proposed switchable microwave photonic filter is shown in Figure 1. A laser diode (LD) is externally modulated by a MZM driven by the microwave signal emitted from the RF port of a vector network analyzer (VNA). An erbium-doped fiber amplifier (EDFA) and an optical attenuator (ATT) are used to control the power of the modulated optical signal, which is split into two paths by an optical coupler (OC1). In one path, the modulated optical signal goes into the photo-detector (PD) directly and realizes an all-pass filter. In the other path, the modulated optical signal enters the RDL loop consisting of two optical couplers (OC1 and OC2), an optical circulator, an RSOA, an OBF, and an OVDL. After coupling into the RDL loop, the modulated optical signal serving as a pump signal is injected into the RSOA via the optical circulator. The ASE of the RSOA is inversely modulated by the pump signal due to the XGM effect, and then the information carried by the pump light is inversely copied onto the ASE at the output of the RSOA. The OBF is used to extract the converted signal, which is a low-coherence ASE signal and serves as a negative tap. The OC2 is employed to take out one part of optical power from the RDL loop, and the other part is reamplified and delayed to obtain the subsequent recursive taps. The converted signal circulating in the RDL loop realizes a high-Q bandpass filter with negative coefficients, and it is obtained at output Port1. On the other hand, the broadband all-pass filter is with positive coefficients. The negative bandpass filter and the broadband all-pass filter are synthesized to achieve a narrow notch filter with flat passband, and it is obtained at output Port2. Thus, the switchability of the filter transfer function is achieved by selecting different output ports. The OVDL is used to adjust the length of the RDL to realize the tunability of the switchable filter. The optical signals processed by the filter are launched into the PD to be converted to electrical microwave signals. The detected signals are sent back to the VNA to measure the frequency response of the filter.

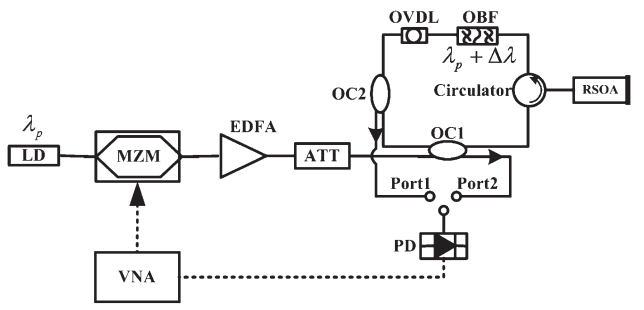

Figure 1 Schematic diagram of the proposed switchable microwave photonic filter. LD, laser diode; MZM: Mach–Zehnder modulator; EDFA, erbium-doped fiber amplifier; ATT, attenuator; OC, optical coupler; RSOA, reflective semiconductor optical amplifier; OBF, optical bandpass filter; OVDL, optical variable delay line; PD, photo-detector; VNA, vector network analyzer

Due to the short coherent length of the modulated ASE signal, the negative bandpass filter obtained at output Port1 will operate in the incoherent domain. The transfer function of the bandpass filter can be simply written as

$$H_{\mathrm{ban}}(\omega) \propto \frac{\eta(1-\kappa_1)(1-\kappa_2)g_c^2 L_c}{1-\kappa_1\kappa_2 g_c^2 L_c e^{-j\omega T_{\mathrm{act}}}} \tag{1}$$

where η represents the XGM conversion coefficient of the microwave signal, κ_1 and κ_2 are the OC1 and OC2 coupling coefficients, respectively, g_c is the effective gain of the converted signal, L_c is the corresponding optical loss coefficient, ω is the modulating angular frequency of the microwave signal, and T_{act} is the time delay of the RDL loop.

The transfer function of the notch filter with flat passband obtained at output Port2 can be expressed by

$$H_{\mathrm{not}}(\omega) \propto \underbrace{\kappa_1}_{H_1(\omega)} \underbrace{- \frac{\eta(1-\kappa_1)(1-\kappa_2)g_c^2 L_c e^{-j\omega T_{\mathrm{act}}}}{1-\kappa_1\kappa_2 g_c^2 L_c e^{-j\omega T_{\mathrm{act}}}}}_{H_2(\omega)} \tag{2}$$

where $H_1(\omega)$ and $H_2(\omega)$ represent the all-pass filter function and bandpass filter function, respectively. It should be noted that the bandpass component is delayed by T_{act} comparing with the all-pass component, and the bandpass component and the all-pass component are out of phase, then correspondingly, there is a phase shift of $e^{-j\omega T_{\mathrm{act}}}$ and a negative sign in the bandpass component comparing with the all-pass component. In addition, as the converted signal and all-pass signal are carried by different wavelength lights, the optical interference between the optical bandpass component and the all-pass component is avoided.

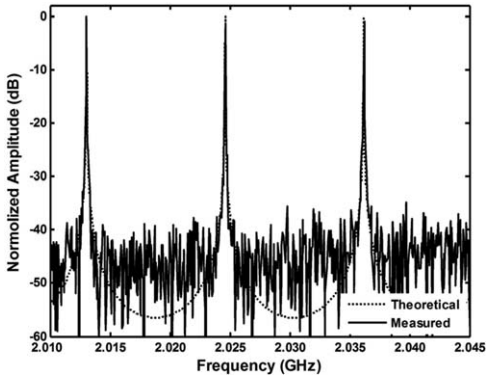

Figure 2 Theoretical and measured bandpass frequency responses

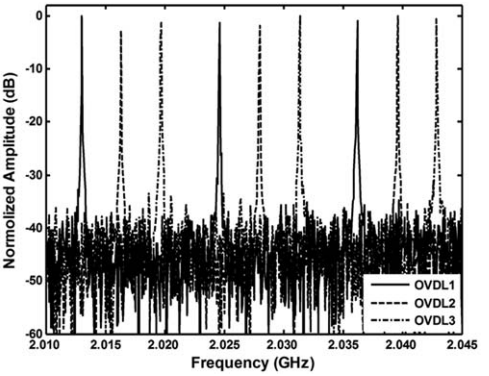

Figure 4 Measured bandpass frequency responses with different time delays of the OVDL

3. EXPERIMENTAL RESULTS AND DISCUSSION

An experiment based on the schematic diagram shown in Figure 1 is carried out. In the experiment, the central wavelength of the LD is 1560 nm. The OBF with a 3 dB bandwidth of 1.2 nm is centered at 1557.8 nm, detuning from the LD central wavelength by 2.2 nm. The OC1 is a 2 × 2 50:50 coupler used to form the RDL loop and split the modulated optical signal. The OC2 is a 1 × 2 10:90 coupler, and it is employed to take out 10% optical power from the RDL loop, while the residual 90% power is kept in the amplified loop and delayed to obtain the subsequent recursive taps. When the PD port is connected to output Port1, and the ATT and the RSOA current are adjusted properly, a high-Q bandpass frequency response is obtained after PD. The theoretical and measured bandpass frequency responses are shown in Figure 2, and they are agreed very well. The measured free spectral range (FSR) is 11.58 MHz, and the 3 dB bandwidth is 65.69 kHz, and then the resulting Q factor is about 176. The rejection ratio is about 40 dB. When the PD port is switched to output Port2, and the RSOA current is adjusted properly again, a deep notch frequency response with flat passband is obtained. The theoretical and measured notch frequency responses are shown in Figure 3. The rejection ratio is about 40 dB, and 3 dB bandwidth is about 863.6 kHz.

For the notch filter, the notch rejection ratio is determined by the relationship between the direct path microwave signal power and the passband power of the bandpass filter response. When the two powers are equal, a maximum deep notch frequency response can be achieved. The notch width is proportional to the width of the microwave bandpass filter. It is noted that the passband of the notch filter is not very flat. This is because the pump signal is not filtered out by the OBF completely, and the pump signal realizes a weak bandpass frequency response. Thus, the overall frequency response of the filter is realized by the subtraction of the two bandpass responses after photodetection. In addition, the shape of the notch frequency response is not symmetric, the reason is that the converted signal is delayed a little relative to the pump signal due to the wavelength conversion process, and then the time delay of the negative bandpass filter realized by the converted signal is a little larger than the delay of the bandpass filter realized by the pump signal. The above characteristics are all considered in the theoretical frequency response, as shown in Figure 3. As can be seen from Figure 3, the theoretical and measured frequency responses are agreed very well.

To demonstrate the tunability of the switchable filter, we decrease the OVDL, whose original time delay is 40 ps. The measured high-Q bandpass frequency response with the OVDL tuned with about 15 ps interval is shown in Figure 4. The OVDL1, OVDL2, and OVDL3 are corresponding to the OVDL with 40, 25, and 10 ps, respectively. And the corresponding measured notch frequency responses with different time delays of the OVDL are shown in Figure 5. The time delays of the OVDL corresponding to OVDL1, OVDL2, and OVDL3 in Figure 5 are the same as the delays of the OVDL in Figure 4. Both the bandpass and the notch frequency responses with a tuning step of about 3.31 MHz are experimentally demonstrated, as shown in Figures 4 and 5, respectively.

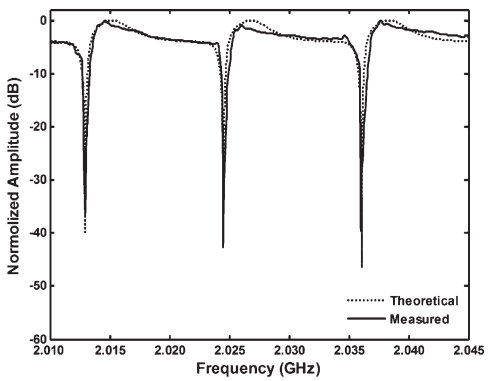

Figure 3 Theoretical and measured notch frequency responses

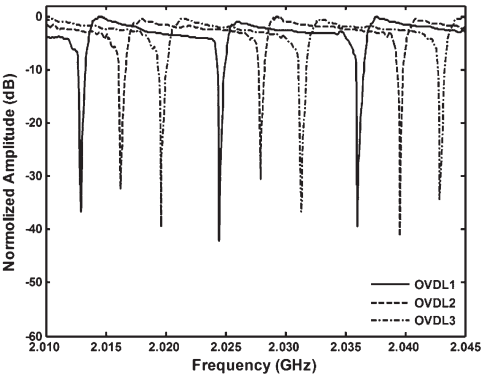

Figure 5 Measured notch frequency responses with different time delays of the OVDL

In addition, the proposed filter structure can simultaneously implement a bandpass filter at Port1 and a notch frequency filter at Port2 by properly choosing the RSOA current and the detuning of the OBF central wavelength from the LD wavelength.

4. CONCLUSION

A novel microwave photonic filter, which can be switched between a high-Q microwave bandpass filter and a notch filter, has been proposed and experimentally demonstrated. The filter is based on a RDL loop with an RSOA followed by an OBF filter. The negative tap is generated by using the wavelength conversion employing the XGM of the ASE in the RSOA. Switching of the filter function between a high-Q bandpass frequency response and a notch frequency response is achieved by changing the output port of the RDL loop. The tunability of the switchable filter is realized by adjusting an OVDL. In addition, the proposed filter structure can simultaneously implement a bandpass frequency response and a notch frequency response at different output ports.

ACKNOWLEDGMENTS

This work was supported in part by the National Natural Science Foundation (No. 61007064), the Jiangsu Natural Science Foundation (No. BK2012432), the Ph.D. Programs Foundation of the Ministry of Education of China (No. 20123223120005), and the Scientific Research Foundation of Nanjing University of Posts and Telecommunications (No. NY211017).

REFERENCES

1. J. Capmany, B. Ortega, and D. Pastor, A tutorial on microwave photonic filters, J Lightwave Technol 24 (2006), 201–229.
2. R.A. Minasian, Photonic signal processing of microwave signals, IEEE Trans Microwave Theory Tech 54 (2006), 832–846.
3. J. Yao, Microwave photonics, J Lightwave Technol 27 (2009), 314–335.
4. C. Pulikkaseril, E.H.W. Chan, and R.A. Minasian, Coherence-free microwave photonic bandpass filter using a frequency-shifting recirculating delay line, J Lightwave Technol 28 (2010), 262–269.
5. E.H.W. Chan and R.A. Minasian, Tunable microwave photonic bandpass filter with high-resolution, coherence-free operation, Electron Lett 47 (2011), 113–115.
6. E.H.W. Chan, Tunable coherence-free microwave photonic bandpass filter based on double cross gain modulation technique, Opt Express 20 (2012), 22987–22996.
7. E.H.W. Chan and R.A. Minasian, High-resolution tunable RF/microwave photonic notch filter with low-noise performance, J Lightwave Technol 29 (2011), 3304–3309.
8. W. Zhang and R.A. Minasian, Ultrawide tunable microwave photonic notch filter based on stimulated Brillouin scattering, IEEE Photon Technol Lett 24 (2012), 1182–1184.
9. E.H.W. Chan and R.A. Minasian, Multiple-tap, tunable microwave photonic interference mitigation filter, J Lightwave Technol 29 (2011), 1069–1076.
10. Y. Yu, E. Xu, J. Dong, L. Zhou, X. Li, and X. Zhang, Switchable microwave photonic filter between high Q bandpass filter and notch filter with flat passband based on phase modulation, Opt Express 18 (2010), 25271–25282.
11. E.H.W. Chan, All-optical reconfigurable microwave photonic signal processor, Microwave Opt Technol Lett 50 (2008), 1989–1991.
12. W. Zhang and R.A. Minasian, Switchable and tunable microwave photonic Brillouin-based filter, IEEE Photon J 4 (2012), 1443–1455.

HIGH SELECTIVITY BAND PASS FILTERS ON ISO/ANISOTROPIC DIELECTRIC, FERRIMAGNETIC, AND METAMATERIAL SUBSTRATES

Valdemir P. Silva Neto, Cristhianne F. L. Vasconcelos, Maria Rosa M. L. Albuquerque, and Adaildo G. D'Assunção
Federal University of Rio Grande do Norte, UFRN-CT-DCO, Caixa Postal 1655, CEP: 59078-970, Natal, Rio Grande do Norte, Brazil; Corresponding author: adaildo@ct.ufrn.br

Received 16 May 2013

ABSTRACT: *This work describes a frequency response investigation of a band pass microstrip filter geometry printed on different substrate materials. The filter geometry comprises a wavelength rectangular ring resonator that is side coupled to two quarter-wavelength lines to provide the access ports. This filter geometry is particularly suitable for high-frequency selective applications. The investigation of the properties of the filter geometry is carried out for iso/anisotropic dielectric, ferrimagnetic, and metamaterial substrates, for comparison purpose. Simulation and design are performed using Ansoft HFSS, a commercial software based on the accurate finite element method. Resonant frequency, return loss, insertion loss, and percent bandwidth results are compared and discussed, taking into account the effect produced by each material substrate on the filter performance. Prototypes of band pass filters on isotropic substrates are built and measured. Simulated and measured results are in agreement.* © 2014 Wiley Periodicals, Inc. Microwave Opt Technol Lett 56:201–206, 2014; View this article online at wileyonlinelibrary.com. DOI 10.1002/mop.28066

Key words: *microstrip ring resonator; band pass filter; high-frequency selectivity; anisotropic dielectric; metamaterial; ferrimagnetic*

1. INTRODUCTION

A microstrip ring resonator has many attractive features such as printed circuit technology fabrication, compact size, and low-cost integration. It holds a great deal of potential applications as basic construction element in the development of filters, couplers, and antennas at microwave and millimeter wave frequencies [1–9].

Over the years, many papers have been devoted to the study of planar filters on isotropic dielectric substrates. Alternatively, a growing interest has been observed in the development of band pass filters supported by anisotropic dielectric [4], metamaterial [10–13], and ferrimagnetic [14,15] substrates to take advantage of the dielectric and magnetic anisotropy effect on the transmission properties of these structures.

Therefore, the aim of this article is to investigate the performance of bandpass filters printed on complex materials and compare their behavior with the bandpass microstrip filters on isotropic substrates. The filter is realized using the configuration illustrated in Figure 1.

The main characteristics such as center frequency, bandwidth (BW), transmission zeros frequencies, and insertion loss of the bandpass filters supported by different materials are presented and discussed. The microstrip filter design uses the synthesis of the ring resonator. Design equations of the proposed structures are given in [3]. It is possible to evaluate various filter parameters, with different configurations and substrates. Results for return loss, insertion loss, center frequency, and BW are simulated by Ansoft HFSS software.